Advances in the computational modeling of the gecko adhesion mechanism

Roger A. Sauer[1]

Emmy-Noether Research Group on Computational Adhesion,
Aachen Institute for Advanced Study in Computational Engineering Science (AICES),
RWTH Aachen University, Templergaben 55, 52056 Aachen, Germany

Published[2] in the *Journal of Adhesion Science and Technology*, DOI: 10.1080/01694243.2012.691792
Submitted on 17 January 2011, Revised on 2 August 2011, Accepted on 16 November 2011

Abstract

This paper provides an overview of recent advances in the computational modeling of the gecko adhesion mechanism. Several efficient modeling approaches are introduced that address the adhesion mechanism at various length scales, ranging from the molecular interaction at the Ångstrom scale to the toe description at the centimeter scale. In particular, detailed three-dimensional models for the gecko spatulae and setae are discussed. The emphasis here is placed on the computational efficiency of the presented contact formulations using coarse-graining and model order reduction. Different finite element methods, based on non-linear structural mechanics, are considered to analyze the resulting models. Both continuum and beam formulations are discussed. In order to obtain an accurate description of peeling, a local finite element surface enrichment technique is presented. The paper also provides some ideas on future modeling approaches.

keywords: computational contact mechanics, enriched finite elements, gecko adhesion, large deformations, multiscale approaches, non-linear finite elements, peeling

1 Introduction

Many insects and lizards, like the tokay gecko, have developed remarkable structural mechanisms to access attractive forces at the molecular scale and translate these into strong adhesional forces at the macroscale. Figure 1 gives an illustration of the adhesion mechanism used by the tokay gecko. The soft tissue of the gecko toes is covered by very fine hairs, the so-called setae, which are only about a hundred micrometers long and a few micrometers thick. The setae branch into even finer hairs, the so-called spatulae, which are about a thousand nanometers long but only a few nanometers thick at their tips. This gives the spatulae great flexibility to adhere to even very rough substrates. The adhesion itself is governed by van der Waals interaction at the molecular scale. Altogether this mechanism spans about nine orders of magnitude (from the Ångstrom scale of the atoms to the decimeter scale of the gecko). The modeling of the entire mechanism poses several major challenges, such as the complex surface microstructure, the non-linear material description of the structures, the contact dynamics of impact and friction, the identification and determination of characteristic model parameters, the instabilities caused by strong adhesion, the peeling behavior of the structure, the model transition between the

[1]Email: sauer@aices.rwth-aachen.de

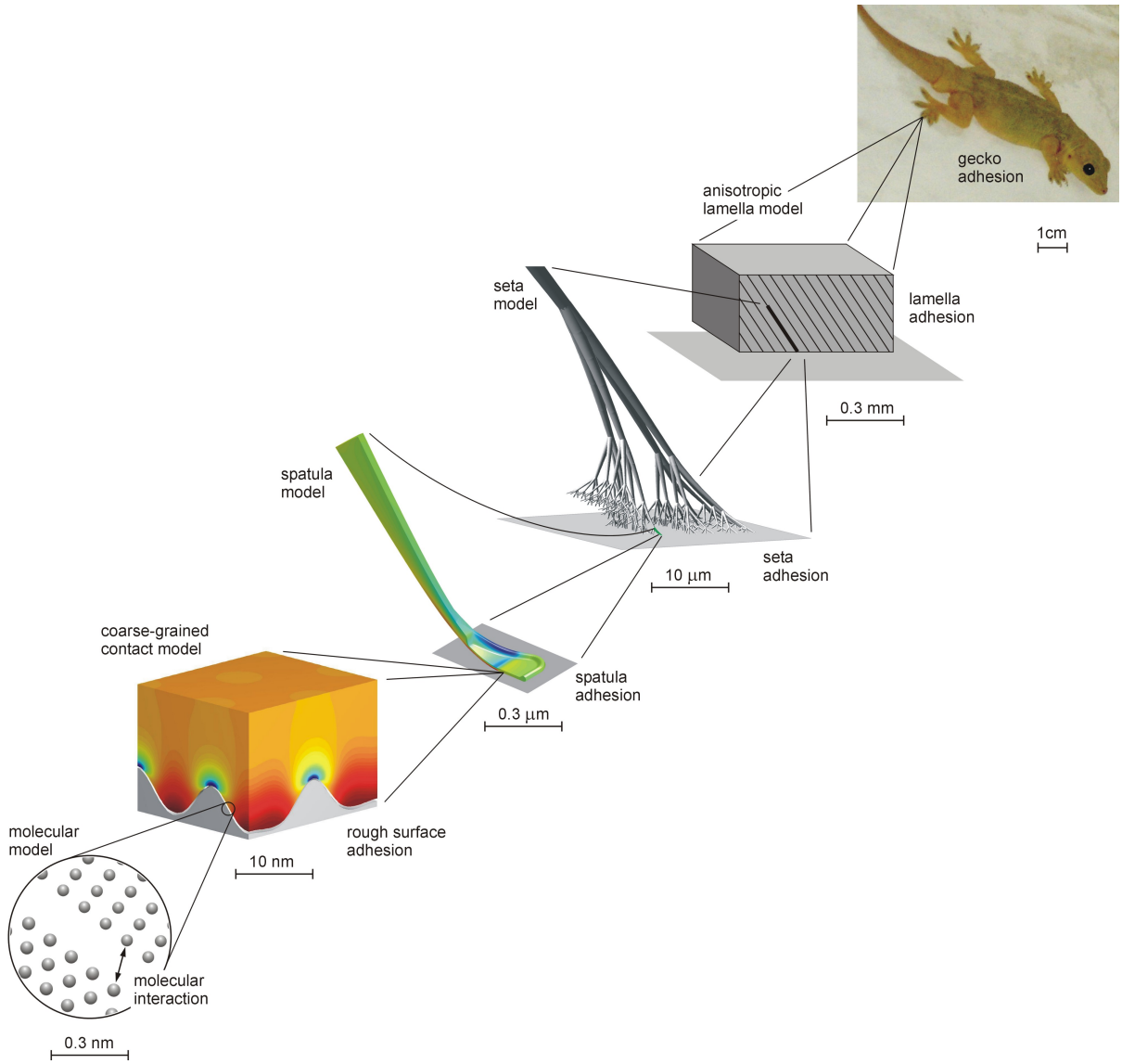

Figure 1: Multiscale modeling hierarchy of the adhesion mechanism used by the gecko

different scales using coarse-graining techniques, the formulation of multiscale models, and the consideration of multifield aspects, like the coupling of mechanical, thermal, chemical and biological aspects (Sauer, 2011a). In order to handle all these complexities, computational models are called for. This paper provides an overview of recent computational advances in the modeling of the gecko adhesion mechanism that address several of these challenges. Since computational approaches are only practical if they are accurate, efficient and stable, the focus is placed on these properties in the following discussion. To the best of the author's knowledge, the models presented here are the only computational approaches reported in the literature that model the gecko adhesion mechanism in detail. A recent overview of analytical modeling approaches is given by Kwaki and Kim (2010). This work also mentions many important experimental studies on gecko adhesion. Further recent experimental studies, that are not covered in this review, are given by Hansen and Autumn (2005); Gravish et al. (2008); Huber et al. (2008); Pugno and Lepore (2008); Chen and Gao (2010); Puthoff et al. (2010); Hill et al. (2011). This list is by no means exhaustive. References that are directly related to the modeling aspects addressed here are mentioned in the corresponding sections below.

Following the modeling levels identified in Figure 1 in a bottom-up approach, Sections 2 to 8 discuss several distinct and independent submodels that address different aspects of the gecko adhesion mechanism. Remarks on top-down modeling are provided in Section 9. Section 10 concludes the paper.

2 Coarse-graining of molecular adhesion

The interaction of neighboring bodies, like contact and adhesion, is caused by the interactions between the individual atoms of these bodies. At very small length scales one can use molecular dynamics to model and compute the behavior of the bodies. This, however, becomes inefficient in the range above several nanometers, so that a coarse-grained description of the interaction is desired. Such a description is presented here for the case of van der Waals adhesion.
Therefore, consider two bodies, denoted $\hat{\mathcal{B}}_1$ and $\hat{\mathcal{B}}_2$, that contain n_1 and n_2 atoms, as shown in Figure 2. Instead of keeping track of all $n_1 + n_2$ particles, an effective continuum model is

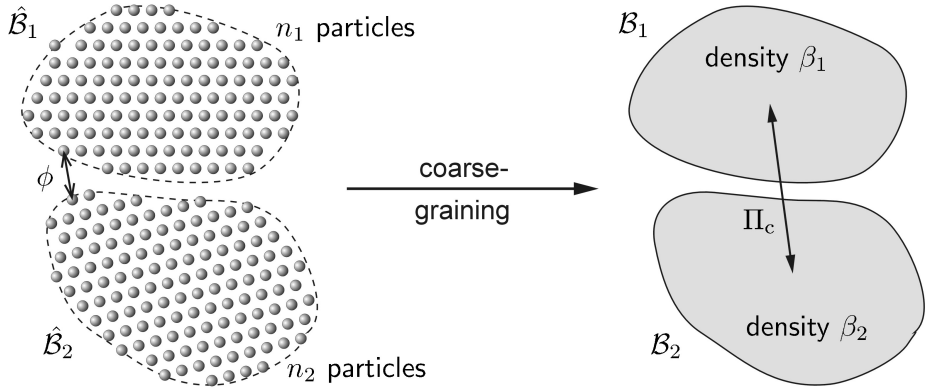

Figure 2: Coarse-graining of the molecular interaction ϕ between the discrete bodies $\hat{\mathcal{B}}_1$ and $\hat{\mathcal{B}}_2$ into the interaction Π_c between the continua $\mathcal{B}_1$ and $\mathcal{B}_2$.

sought, that provides an overall interaction formulation. The van der Waals interaction between two particles, separated by r, can be described by the Lennard-Jones potential

$$\phi(r) := \epsilon\Big(\frac{r_0}{r}\Big)^{12} - 2\epsilon\Big(\frac{r_0}{r}\Big)^{6} , \tag{1}$$

where ϵ and r_0 are model constants. The total interaction energy between the two bodies is then given by the summation

$$\hat{\Pi}_c = \sum_{i=1}^{n_1}\sum_{j=1}^{n_2} \phi(r_{ij}) , \quad \text{with} \quad r_{ij} = \|\mathbf{x}_i - \mathbf{x}_j\| . \tag{2}$$

In the continuum setting the double summation is replaced by the double integration over the volume of the two bodies, i.e.

$$\Pi_c = \int_{\mathcal{B}_1}\int_{\mathcal{B}_2} \beta_1\,\beta_2\,\phi(r)\,\mathrm{d}v_2\,\mathrm{d}v_1 , \quad \text{with} \quad r = \|\boldsymbol{x}_1 - \boldsymbol{x}_2\| , \quad \boldsymbol{x}_k \in \mathcal{B}_k . \tag{3}$$

Here, β_k $(k = 1, 2)$ denotes the current particle density of $\mathcal{B}_k$, i.e. the density of the atoms in the deformed configuration of the bodies. The current density β_k is related to the reference density β_{0k} (the density in the undeformed configuration of the bodies, denoted $\mathcal{B}_{0k}$, $k = 1, 2$) via the

volume change during deformation. Considering conservation of mass during deformation, the identity

$$\beta_k \, \mathrm{d}v_k = \beta_{0k} \, \mathrm{d}V_k \tag{4}$$

holds. Here, $\mathrm{d}v_k$ and $\mathrm{d}V_k$ denote differential volume elements in the deformed and undeformed configurations, respectively. With this, expression (3) can also be written as

$$\Pi_\mathrm{c} = \int_{\mathcal{B}_{01}} \int_{\mathcal{B}_{02}} \beta_{01} \, \beta_{02} \, \phi(r) \, \mathrm{d}V_2 \, \mathrm{d}V_1 \ . \tag{5}$$

The distance $r = \|\boldsymbol{x}_1 - \boldsymbol{x}_2\|$ between two material points $\boldsymbol{x}_1 \in \mathcal{B}_1$ and $\boldsymbol{x}_2 \in \mathcal{B}_2$ refers to the deformed configurations of the bodies. These are obtained from the deformation mapping $\boldsymbol{x}_k = \boldsymbol{\varphi}_k(\boldsymbol{X}_k)$ of the reference points $\boldsymbol{X}_k \in \mathcal{B}_{0k}$.
In order to construct finite element formulations for this adhesion model, the variation of Π_c, the so-called virtual work of interaction, is needed. It can be found as (Sauer and Li, 2007)

$$\delta\Pi_\mathrm{c} = -\sum_{k=1}^{2} \int_{\mathcal{B}_k} \delta\boldsymbol{\varphi}_k \cdot \beta_k \, \boldsymbol{b}_k \, \mathrm{d}v_k \ , \tag{6}$$

where $\boldsymbol{b}_k$ denotes a body force field acting at $\boldsymbol{x}_k \in \mathcal{B}_k$. This field is given by

$$\boldsymbol{b}_k = -\frac{\partial}{\partial \boldsymbol{x}_k} \int_{\mathcal{B}_\ell} \beta_\ell \, \phi \, \mathrm{d}v_\ell \ , \quad \ell \neq k \ . \tag{7}$$

A finite element formulation, which is directly applied to this formulation, is given in Sauer and Li (2007). Due to the required six levels of integration (in 3D) such direct formulations tend to be very inefficient for most applications. Therefore, the following section discusses further coarse-graining steps to increase the efficiency of computational formulations. In principle, the formalism described above can also be used to describe other interaction mechanisms.

3 Efficient computational formulations for nanoscale adhesion

This section discusses efficient finite element formulations for evaluating the contact energy $\delta\Pi_\mathrm{c}$ for nanoscale adhesion. The basic idea is to reduce the amount of numerical integration by introducing analytical approximations.
The first such approach is to approximate integration (7). This is achieved by considering the following two steps: In order to evaluate the body force $\boldsymbol{b}_k$ at a given point $\boldsymbol{x}_k \in \mathcal{B}_k$, one first computes the minimum distance between $\boldsymbol{x}_k$ and the neighboring surface $\partial\mathcal{B}_\ell$, i.e.

$$r_k = \min_{\forall \boldsymbol{x}_\ell} \|\boldsymbol{x}_k - \boldsymbol{x}_\ell\| \ , \quad \boldsymbol{x}_\ell \in \partial\mathcal{B}_\ell \ . \tag{8}$$

The closest point to $\boldsymbol{x}_k$ on $\partial\mathcal{B}_\ell$ is denoted $\boldsymbol{x}_\mathrm{p}$ and the surface normal at $\boldsymbol{x}_\mathrm{p} \in \partial\mathcal{B}_\ell$ is denoted $\boldsymbol{n}_\mathrm{p}$, as shown in Figure 3 below. Secondly, one approximates the neighboring body $\mathcal{B}_\ell$ at point $\boldsymbol{x}_\mathrm{p}$ by a flat half-space and integrates eq. (7) analytically. One thus obtains (Sauer and Wriggers, 2009)

$$\boldsymbol{b}_k = \pi\beta_\ell\epsilon r_0^2 \left[\frac{1}{5}\left(\frac{r_0}{r_k}\right)^{10} - \left(\frac{r_0}{r_k}\right)^{4}\right] \boldsymbol{n}_\mathrm{p} \ . \tag{9}$$

The constants appearing here can be replaced by Hamaker's constant $A_H = 2\pi^2\beta_{01}\beta_{02}\epsilon r_0^6$ (Israelachvili, 1991). Compared to eq. (7), approximation (9) is much more efficient to evaluate. Sauer and Wriggers (2009) have shown that the accuracy of this approximation is very good if the surface curvature radii of $\partial\mathcal{B}_\ell$ are larger than 8 nm.

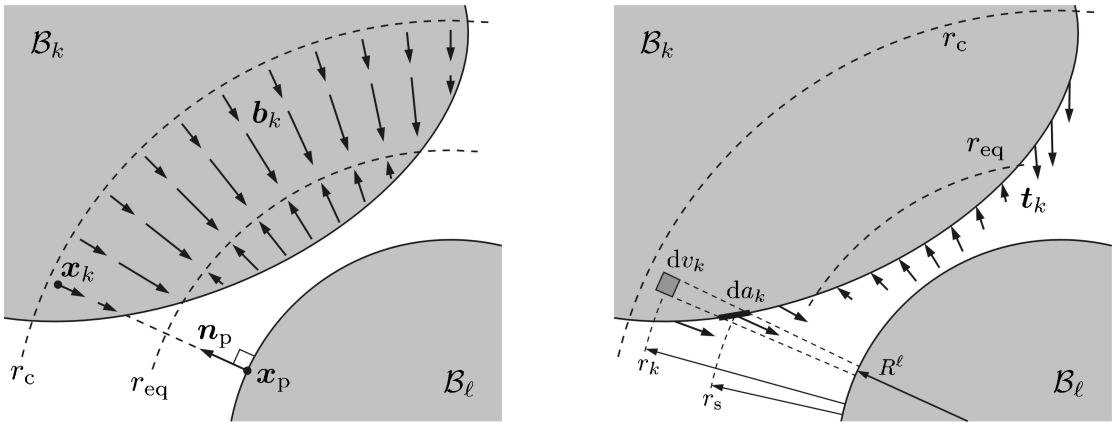

Figure 3: Minimum distance computation between $\boldsymbol{x}_k$ and $\partial\mathcal{B}_\ell$ used to evaluate the body forces $\boldsymbol{b}_k(\boldsymbol{x}_k)$ (left); Replacement of the body forces by an effective surface traction $\boldsymbol{t}_k$ (right); (Sauer and Wriggers, 2009).

The second approach considers the approximation of the virtual work computation in eq. (6). Since the body force field $\boldsymbol{b}_k$ is concentrated along the surface of body $\mathcal{B}_k$, it is useful to replace $\boldsymbol{b}_k$ by an effective surface traction $\boldsymbol{t}_k$.[3] This traction is obtained by the projection of all body forces along direction $-\boldsymbol{n}_\mathrm{p}$ onto the surface $\partial\mathcal{B}_k$, as shown in Figure 3. Considering eq. (9), the effective surface traction

$$\boldsymbol{t}_k = \pi\beta_k\beta_\ell\epsilon r_0^3\left[\frac{1}{45}\left(\frac{r_0}{r_\mathrm{s}}\right)^9 - \frac{1}{3}\left(\frac{r_0}{r_\mathrm{s}}\right)^3\right]\boldsymbol{n}_\mathrm{p}\ , \tag{10}$$

is thus obtained. The distance r_s is obtained from eq. (8) considering that now also $\boldsymbol{x}_k$ is a surface point ($\boldsymbol{x}_k \in \partial\mathcal{B}_k$). In Sauer and Wriggers (2009) the difference between the body force formulation (9) and the surface traction formulation (10) is investigated and it is found that a significant difference appears only for materials that are much softer than beta-keratin, which is the material of the gecko foot-hairs. It is noted, that both formulations are locally normal contact models. Tangential contact forces can be introduced by other mechanisms, as is discussed in Sec. 5.
The virtual contact work can now be written as

$$\delta\Pi_\mathrm{c} \approx -\sum_{k=1}^{2}\int_{\partial\mathcal{B}_k}\delta\boldsymbol{\varphi}_k\cdot\boldsymbol{t}_k\cos\alpha_k\,\mathrm{d}a_k\ . \tag{11}$$

Here the angle α_k describes the inclination between the two neighboring surfaces at $\boldsymbol{x}_k$. The finite element vector, which captures the contact forces acting on the finite element nodes, then follows as

$$\mathbf{f}_{ck}^e = -\int_{\Gamma_k^e}\mathbf{N}_k^T\,\boldsymbol{t}_k\,\cos\alpha_k\,\mathrm{d}a_k\ , \tag{12}$$

where $\mathbf{N}_k$ is an array that contains the shape functions of the finite element nodes. It is noted that the integral over the current surface $\partial\mathcal{B}_k$ can be transformed to an integral over the reference surface $\partial\mathcal{B}_{0k}$ (Sauer and Wriggers, 2009). The finite element stiffness matrix corresponding to $\mathbf{f}_{ck}^e$ can be found in Sauer (2012a).
A significant gain in CPU time can be achieved from approximations (9) and (10); see Sauer and

[3] Beyond a distance of 5.7 nm, the magnitude of $\boldsymbol{b}_k$ is less than 0.1% of its maximum attraction value. This distance is less than the thickness of the gecko spatula.

Li (2008). They also lead to more stable finite element formulations (Sauer, 2006). Standard displacement based finite elements can be used to evaluate eq. (12). However, for problems extending into the micrometer range, standard contact finite elements are quite inefficient, so that it is highly advantageous to consider special element formulations for adhesion, as are described in the following section.

4 Efficient formulations for adhesion: Enhanced contact finite elements

This section presents a finite element enrichment technique for contact computations, which is more accurate, stable and efficient than standard finite element discretization approaches. The enrichment approach, originally presented in Sauer (2011b), is motivated by the fact that during adhesive contact sharp peeling stress peaks often occur at the peeling front. The basic idea, therefore, is to enrich the surface elements such that the finite element approximation is more accurate on the surface than it is in the bulk. The simplest of these is the so-called Q1C2 element, which approximates the contact surface by a quadratic interpolation while the bulk is approximated by a linear interpolation. This formulation has the same contact accuracy as a fully quadratic finite element contact description, but is much more efficient. The Q1C2 element is combined with a standard linear finite element (FE) interpolation formulation within the bulk (like the Q1 element formulation), so that the interpolation is fully quadratic on the contact surface $\partial_c \mathcal{B}^h$ but only linear in the bulk $\mathcal{B}^h$. Formally this can be written as

$$\begin{array}{ll} \boldsymbol{u}^h \in \mathcal{P}^1 & \text{in } \mathcal{B}^h \ , \\ \boldsymbol{u}^h \in \mathcal{P}^2 & \text{on } \partial_c \mathcal{B}^h \ , \end{array} \tag{13}$$

where $\mathcal{P}^1$ denotes the space of continuous, piecewise linear interpolation functions and $\mathcal{P}^2$ denotes the space of continuous, piecewise quadratic interpolation functions. Considering standard 8-noded linear brick elements, five additional enrichment nodes are required on the contact surface of the element in order to satisfy condition (13) as Figure 4 shows. The finite element

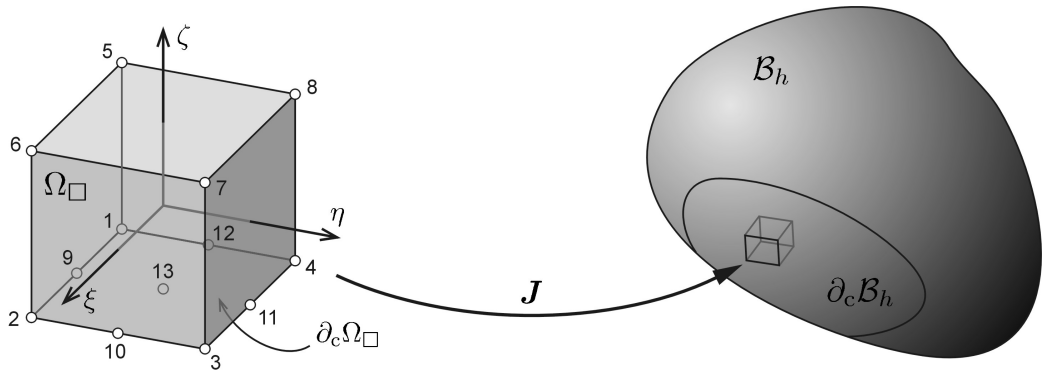

Figure 4: 3D surface enrichment based on p-refinement: 3D enhanced contact element Q1C2 and its map to the current domain (Sauer, 2011b).

approximation of the displacement field $\boldsymbol{u}$ within the element is then given by the nodal interpolation

$$\boldsymbol{u}_e^h = \sum_{I=1}^{13} N_I \, \mathbf{u}_I \ , \tag{14}$$

where N_I $(I = 1, ..., 13)$ denote the shape functions associated with the 13 nodes; see Sauer (2011b) for details. The Q1C2 formulation already achieves a substantial gain in computational accuracy and stability, however, the improvement becomes even better in the following approach.

Another enrichment idea consists in using Hermite interpolation on the contact surface, but using standard linear interpolation in the bulk, such that the interpolated displacement field $\boldsymbol{u}^h$ is continuous (C^0) in the entire domain, $\mathcal{B}^h$, and continuously differentiable (C^1) on the entire contact surface, $\partial_c \mathcal{B}^h$, i.e.

$$\begin{aligned} \boldsymbol{u}^h &\in C^0 \quad \forall\, \boldsymbol{x} \in \mathcal{B}^h \ , \\ \boldsymbol{u}^h &\in C^1 \quad \forall\, \boldsymbol{x} \in \partial_c \mathcal{B}^h \ . \end{aligned} \tag{15}$$

This is achieved by enriching the finite element nodes on the contact surface by an approximation for the surface derivative. Considering a standard 4-noded quad-element, the enriched FE interpolation takes the form

$$\boldsymbol{u}_e^h = \sum_{I=1}^{4} N_I \, \mathbf{u}_I + \sum_{I=1}^{2} H_I \, \mathbf{u}_{I,S} \ , \tag{16}$$

where $\mathbf{u}_{I,S}$ denotes the derivative at the FE node I of the displacement vector $\boldsymbol{u}$ along the surface coordinate S. The shape functions N_I and H_I, as well as details on the implementation of this element formulation, are provided in Sauer (2011b). This enrichment technique is denoted as the Q1CH formulation. The improved accuracy gained by the Q1CH formulation is illustrated in Figure 5. Sauer (2011b) shows that the error in such peeling computations can be reduced

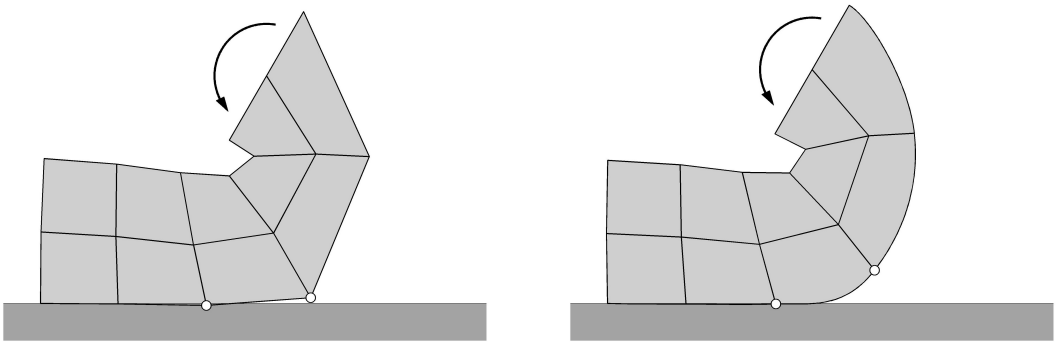

Figure 5: Peeling of an initially flat elastic strip: computation with common Q1C1 contact elements (left); computation with enriched Q1CH contact elements (right). The accuracy gain is particularly large at the peeling front between the marked finite element nodes.

by a factor of 15 compared to the original Q1C1 formulation. The enrichment formulation also shows substantially improved behavior for sliding contact computations. The enriched contact element formulation allows an efficient computation of the peeling behavior of gecko spatulae as is shown in the following section.

5 A detailed 3D model for the gecko spatula

The computational modeling framework outlined in the previous sections allows an efficient simulation of the adhesional behavior of gecko spatulae, which is considered here. In particular, the modeling framework is ideal to study the detailed attachment and detachment behavior of the spatula accounting for variations in spatula size, spatula stiffness, strength of adhesion,

range of adhesion, surface roughness and loading conditions, and to further investigate geometry and material optimization. Such a model and study are considered in Sauer and Holl (2012). There, a three-dimensional description of the spatula shape is presented that is based on twelve parameters and allows to easily consider size and shape variations. As seen in Figure 6, the

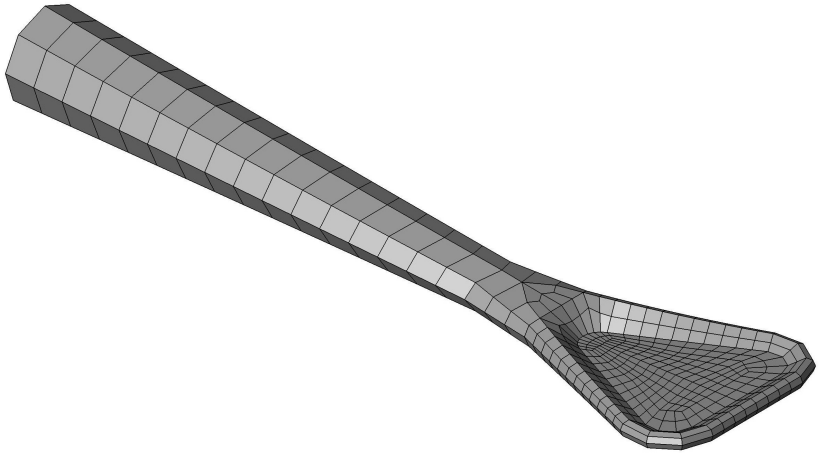

Figure 6: 3D finite element model for a gecko spatula (Sauer and Holl, 2012). The actual finite element mesh used for the computations is much denser than the one shown here.

model considers a detailed description of the spatula pad and its connection to the spatula shaft. The spatula pad is very thin in the middle to give it high flexibility to adapt and attach to rough substrates, but it is surrounded by a thick rim, probably to give it increased stability. The geometry description is based on the microscopic images found in the literature; e.g. see Rizzo et al. (2006). A finite element discretization of the spatula geometry is chosen (see Figure 6) that uses enhanced contact elements (see Sec. 4) and thus provides high accuracy in the evaluation of the contact forces acting on the spatula pad.

Figure 7 shows the results of a pull-off computation. For this, a displacement normal to the substrate surface is applied to the end face of the shaft. The rotation of the spatula end face is considered fixed. The peeling deformation of the spatula is shown on the left, the pull-off force, as a function of the applied displacement, is shown on the right. As seen, the maximum pull-off force obtained from the computation is 6.7 nN, which falls into the range measured by Huber et al. (2005) and Sun et al. (2005).[4] In Sauer and Holl (2012) also several other load conditions, material parameters and geometry parameters are examined. The study shows that the spatula can function over a wide range of model parameters.

The detailed spatula model can also be used to study the influence of substrate roughness. Figure 8 shows the results of such a computation. A periodic roughness structure is considered as is shown on the right. The height of the asperities is taken as 8 nm, the distance between the asperities is 100 nm. The study shows that there can be intimate contact between spatula pad and substrate even in the valleys of relatively rough substrate surfaces. The spatula model is suitable to study the peeling behavior for different pull-off angles and surface roughnesses. Therefore, it is generally necessary to include frictional contact formulations. These can be modeled by tangential contact models (Laursen, 2002; Wriggers, 2006) or by dissipative material models (Wriggers and Reinelt, 2009).

The spatula model presented here requires about 100,000 finite elements to capture the spatula behavior accurately. In some cases, especially at larger length scales, only the overall behavior

[4]The computational result is obtained from the frictionless contact formulation outlined in the previous sections. It is shown in Sauer and Holl (2012) that accounting for frictional contact forces hardly affects the behavior for vertical loading.

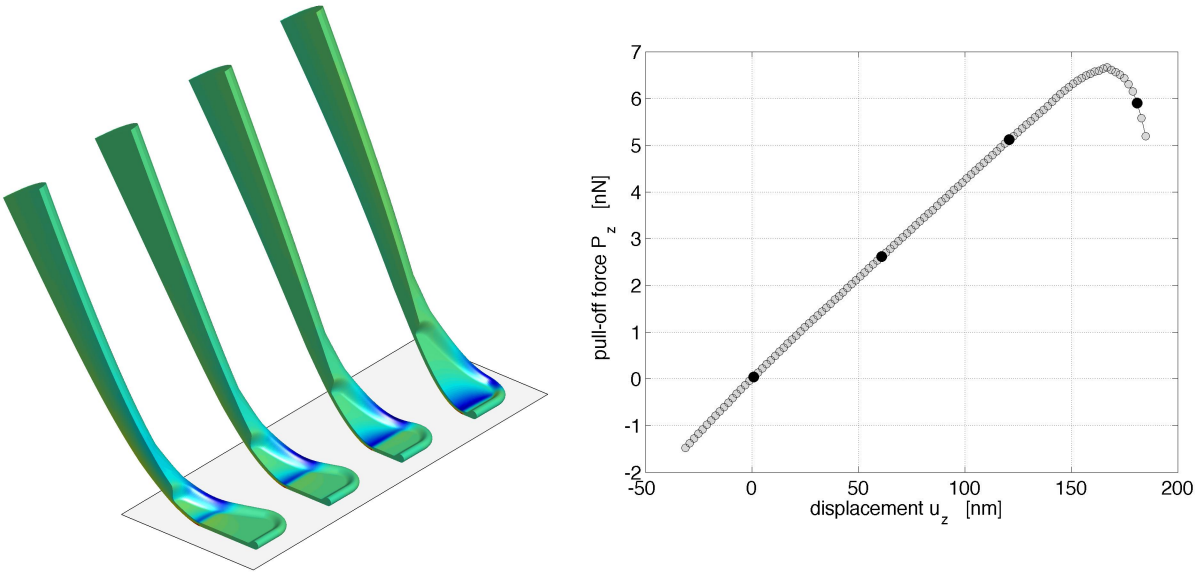

Figure 7: Pull-off simulation of a gecko spatula (Sauer and Holl, 2012): deformed spatula configurations (left; due to symmetry only half of the spatula is shown); normal pull-off force due to a normal displacement applied to the end face of the spatula shaft (right); The four black dots mark the configurations shown on the left.

of the spatula is of interest, and therefore it is desirable to find reduced spatula models that capture the effective adhesion behavior, but require far less computational effort. Such reduced models are discussed in the following section.

6 Reduced beam formulations for adhesion structures

The gecko spatula and seta are relatively thin and elongated structures. The overall behavior of such structures can be described efficiently with beam formulations, which are discussed here. Such formulations are, for example, ideal for the development of computational models for large patches of seta arrays. In this section we focus on reformulating the adhesion model of Sections 2 and 3 for beam structures. The modeling of gecko setae and seta patches is then discussed in the following two sections.

Beam theories are reduced order models that are characterized by the behavior along the beam axis, while the behavior across the cross section is simplified. Therefore, the body force field $\boldsymbol{b}_k$, derived in Sections 2 and 3 for van der Waals adhesion, needs to be replaced by an effective line force acting along the center axis of the beam. Since the beam axis in not necessarily parallel to the substrate surface (e.g. during peeling) an additional distributed bending moment appears, as is shown in Sauer (2011c). The distributed line force and bending moment are obtained from the integration of the body force across the height of the beam. Considering approximation (9), we find the following expression for the distributed contact line force, acting in the direction normal to the substrate surface:

$$\boldsymbol{T}_{\mathrm{c}} = T_{\mathrm{c}}\,\boldsymbol{n}_{\mathrm{p}} = \big(T(r_1) - T(r_2)\big)\,\boldsymbol{n}_{\mathrm{p}} / \cos\theta \;, \tag{17}$$

with

$$T(r) = \frac{A_{\mathrm{H}}}{2\pi r_0^3}\left[\frac{1}{45}\left(\frac{r_0}{r}\right)^9 - \frac{1}{3}\left(\frac{r_0}{r}\right)^3\right] \;, \tag{18}$$

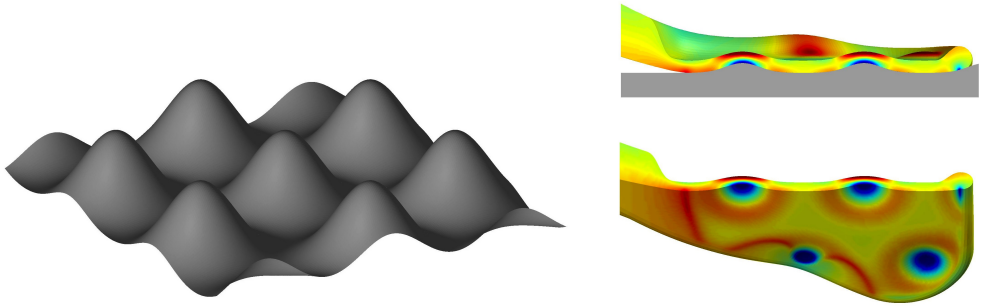

Figure 8: Adhesion of the spatula pad to a rough substrate surface (Sauer and Holl, 2012): surface model (left); deformation of the spatula pad (top right: side view with substrate surface; bottom right: bottom view).

and

$$r_1 = r_\mathrm{M} - \frac{h}{2}\cos\theta \ , \quad r_2 = r_\mathrm{M} + \frac{h}{2}\cos\theta \ . \tag{19}$$

Here h denotes the height of the beam, θ denotes the angle between beam axis and substrate, and r_1, r_M and r_2 denote the distances from the substrate surface to the bottom surface of the beam, beam axis and top surface of the beam, respectively (Sauer, 2011c). A_H and r_0 are the material constants introduced in Sections 2 and 3. The distributed contact bending moment is obtained as

$$M_\mathrm{c} = \left(r_\mathrm{M}\, T_\mathrm{c} - r_0\, T_\mathrm{c}^*\right) \tan\theta \ , \tag{20}$$

with

$$T_\mathrm{c}^* = \left(T^*(r_1) - T^*(r_2)\right) \big/ \cos\theta \ , \tag{21}$$

and

$$T^*(r) = \frac{A_\mathrm{H}}{2\pi r_0^3}\left[\frac{1}{40}\left(\frac{r_0}{r}\right)^8 - \frac{1}{2}\left(\frac{r_0}{r}\right)^2\right] . \tag{22}$$

In most applications we can neglect the contributions $T(r_2)$ and $T^*(r_2)$. The influence of the bending moment is particularly large if the bending deformations during peeling are very large (Sauer, 2011c). The virtual contact work is now given by the virtual work done by $\boldsymbol{T}_\mathrm{c}$ and M_c, i.e.

$$\delta\Pi_\mathrm{c} = -\int_L \left(\delta\boldsymbol{u}\cdot\boldsymbol{T}_\mathrm{c} + \delta\theta\cdot M_\mathrm{c}\right) b\,\mathrm{d}S \ , \tag{23}$$

where L denotes the length of the structure, $\boldsymbol{u}$ and θ denote the displacement and rotation of the cross section and $b(S)$ denotes the width of the contact surface. It is advantageous to consider θ as an independent variable, as is done in the Timoshenko beam theory. This yields a symmetric FE stiffness matrix; see Sauer (2012b). Expression (23) can be applied to any beam formulation. Particularly useful for large deformations are geometrically exact beam formulations, e.g. see Reissner (1972) and Wriggers (2008). In this case, the expression for the FE contact force vector associated with eq. (23) can be found in Sauer (2012b).

Figure 9 shows the deformation during peeling of an elastic strip with a constant height of $h = 10\,\mathrm{nm}$ and elastic modulus of $E = 2\,\mathrm{GPa}$. The adhesion parameters are chosen as $A_\mathrm{H} = 10^{-19}\,\mathrm{J}$ and $r_0 = 0.4\,\mathrm{nm}$.[5] The beam model can be used to investigate the effect of the bending stiffness on the peeling force, as shown in Figure 10 (Sauer, 2011c): For very low stiffness values, the peeling force approaches the result according to Kendall (1975). For larger stiffness values, as we have for the gecko spatula, the computed peeling force disagrees with the Kendall result,

[5]For these parameters, the adhesion energy is $w_\mathrm{adh} = \sqrt[3]{15}A_\mathrm{H}/(16\pi r_0^2) = 0.0307\,\mathrm{J/m^2}$.

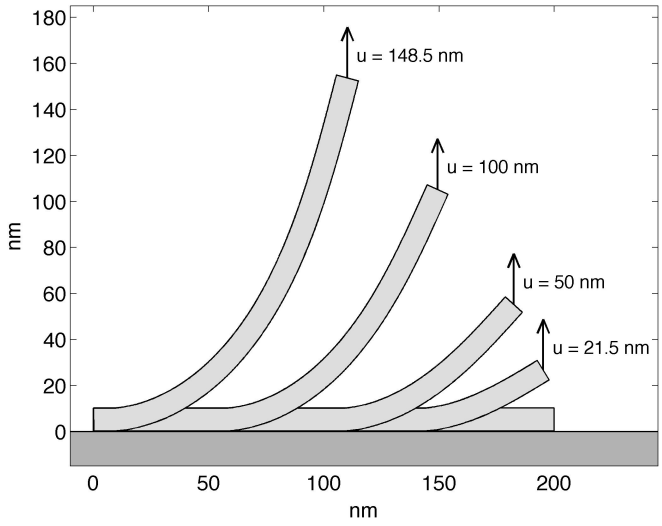

Figure 9: Peeling of a thick elastic strip by an applied vertical displacement u (Sauer, 2011c). The strip is modeled as a non-linear beam. The right end is considered free to rotate and move horizontally, i.e. there is no moment and horizontal force acting at this boundary.

since the Kendall model neglects the bending stiffness of the strip. The unsuitability of the Kendall model for gecko spatulae can also been seen from the detailed 3D spatula computation shown in Figure 7: The spatula peeling force increases gradually, while the Kendall model would predict a constant value. In Sauer (2011c) it is further shown that the spatula stiffness lies in the range where the peeling work attains a maximum. In Sauer (2012b) it is shown that the beam formulation captures the overall peeling behavior of the gecko spatula quite well.

7 A detailed 3D model for the gecko seta

A beam formulation can also be used to describe the behavior of the gecko seta, which is discussed in this section. The challenges in modeling the gecko seta lie in the complex geometry, the constitutive behavior of the fibrilar material, and the effective adhesion behavior of the seta tips. A three-dimensional model for the seta geometry that captures the detailed branching of the hierarchical microstructure but only uses a few geometrical parameters is proposed in Sauer (2009), see Figure 11. In this model, the adhesion behavior at the seta tips is obtained by coarse-graining the adhesion behavior of the spatula, which, in turn, is obtained by a preceding computation at the spatula level. This coarse-graining step is highly useful since it avoids refining the seta tips down to nanoscale resolution in order to capture the adhesion forces given by eqs. (17) and (20). Due to this coarse-graining, the entire seta can be described accurately using only about 1700 finite elements. The seta structure itself is described by a three-dimensional, geometrically exact, non-linear beam formulation (Simo, 1985; Simo and Vu-Quoc, 1986) considering a linear elastic isotropic material response. A difficulty in the coarse-graining, however, is the consideration of model variations at the spatula level, since they may each result in different coarse-grained models. This is further complicated by the non-linearity of adhesion. A useful approach avoiding these difficulties would be to use adaptive coarse-graining, applied only to selected contact regions, during computation. In Sauer (2010) the seta model is used to study the normal pull-off behavior considering different pull-off rates. The maximum pull-off forces obtained from these computations are in the range of 0.4 μN and

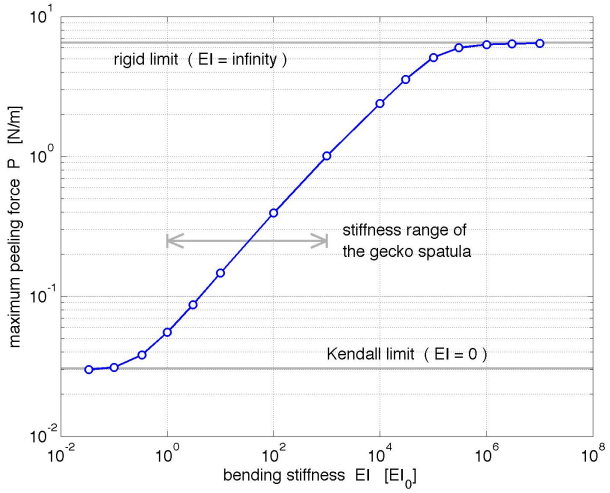

Figure 10: Maximum peeling force of an elastic strip for different values of its bending stiffness EI (Sauer, 2011c). The approximate stiffness range of the gecko spatula is indicated. The bending stiffness (per unit width) is normalized by $EI_0 = Eh^3/12$ with $E = 2\,\mathrm{GPa}$ and $h = 10\,\mathrm{nm}$.

1.4 μN. During pull-off, the seta tips detach successively from the substrate as is shown in Figure 11. Due to its efficiency, the proposed seta model can be used to study the attachment

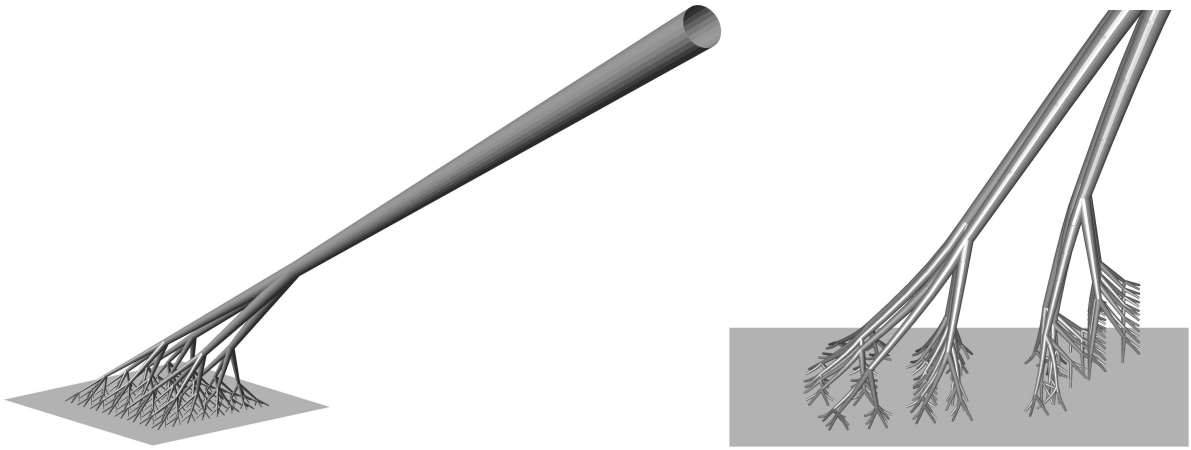

Figure 11: 3D beam model of a gecko seta (left); seta deformation during normal pull-off from an adhering substrate (right) (Sauer, 2009).

and detachment behavior of the seta for various loading conditions, material parameters and geometrical parameters. Given a model for the seta behavior, one can complete the bottom-up modeling of the gecko toe, as is discussed in the following section.

8 Effective adhesion models at the gecko toe level

Each gecko toe is covered with hundreds of thousands of setae, so that the effective adhesion behavior at the toe depends on the combined effect of all these setae. Examining the toes

carefully shows that setae are arranged in lamellas that cover the toes in stripes. Each toe has about a dozen such lamellas. Each lamella consists of a thin flexible band that spans the width of the toe. So far computational approaches to describe the adhesion at the lamella or toe scale have not been formulated. This section, therefore, provides some thoughts on this open research topic.

Due to the alignment of the setae, it can be expected that the adhesion behavior of the lamella and the toe surface is anisotropic, i.e. directionally dependent. This basic property should be reflected by effective lamella and toe models; see Figure 1. In accordance with the bottom-up modeling considered so far, the effective lamella behavior can be obtained from coarse-graining a large patch of setae. For this, one must not only account for the deformation and adhesion properties of each seta, but also account for the effective interaction between neighboring setae. Due to the flexibility of the setae one should also account for the large displacements, rotations and deformations, for example during buckling, of the individual setae in the patch. Due to this, the alignment of the setae may substantially change during deformation. Therefore it may not be sufficient to consider anisotropic continuum models with fixed directions of anisotropy. At present, it seems useful to consider the following coarse-graining steps:

1. Coarse-graining of a seta patch based on a detailed model (e.g. the model discussed in the preceding section) into an effective seta patch, which neglects details like the seta branching, but still accounts for the fibrillar nature of the seta. The coarse-grained seta patch could be described efficiently by a coarse beam formulation.
2. Coarse-graining of the coarse seta patch model into an effective, anisotropic continuum, which could then be described by solid finite elements. At this level one must expect a fairly poor description of local effects such as seta buckling and self-contact.
3. Further coarse-graining of the continuum lamella model into an effective surface adhesion formulation that describes the surface forces acting on the toe by a force-distance relation, similar to the case of van der Waals interaction given in expression (10). Such a formulation would not account for any details of the setae, nor would it account for the details of the spatulae, surface roughness or molecular interaction, but it would still take the effective behavior of all these into account.

9 Top-down modeling: Going all the way back down

In order to provide accurate boundary conditions and far-field conditions for the individual model levels and in order to refine these, one also has to think about top-down modeling. For example, the boundary or loading conditions of the lamella are determined by the dynamics of the toe during gecko locomotion. In turn the dynamics of the lamella provides boundary conditions at the seta level; and so forth. This feedback can be used to refine the individual submodels iteratively, for example in a staggered multiscale approach. As a further idea one can also envision concurrent multiscale strategies that integrate all modeling levels in a coupled computational model. A key requirement to make this as efficient as possible is to consider adaptive modeling strategies that only consider the use of refined model levels for those surface areas that require them. As an example, for the seta detachment shown in Figure 11, it would be advantageous to consider a refined adhesion model only for those seta tips, which are in the process of detachment, while using a coarse description for all other tips. Such approaches, while challenging to set up, may provide the right balance between accuracy and efficiency.

10 Conclusion

This paper discusses the computational modeling of the gecko adhesion mechanism shown in Figure 1. This mechanism spans nine orders of magnitude and therefore cannot be addressed by a single model, but must rather be approached by a combination of several separate but related submodels, which describe different aspects at the various length scales. Considering a bottom-up modeling approach, this paper outlines several detailed three-dimensional adhesion models for deformable continua, gecko spatulae and setae, and gives some ideas on modeling the adhesion behavior at the surface of the gecko toes. In all cases the emphasis is placed on the development of efficient computational formulations. These are based on the introduction of half-space approximation, effective surface tractions, enriched contact finite elements, and reduced beam formulations.
Some of the presented submodels and computational techniques will benefit from further refinement: The enriched contact element technique has not yet been formulated for two deformable bodies, efficient time-integration approaches for adhesion need to be developed, contact algorithms for coupled adhesion and friction are needed, both the spatula and seta models should be revisited, and computational models at the lamella and toe level are still lacking. Also missing is a concurrent multiscale approach combining the different modeling layers into a single simulation framework. With an improved computational modeling framework the pull-off studies at the spatula and seta levels should be re-examined for different roughness and loading parameters. A difficulty in all the modeling approaches discussed here are the uncertainties of the model parameters, like the detailed geometry of the microstructure and the material parameters characterizing large-deformation elasticity and visco-elasticity. These uncertainties call for further experimental studies. Despite these current limitations, computational approaches are the only choice for examining many aspects in detail that are not accessible experimentally and are also the key to conduct optimization studies of the adhesion mechanism, like shape, size and material optimization.

Acknowledgement

The author is grateful to the German Research Foundation (DFG) for supporting this research under project SA1822/5-1 and grant GSC 111.

References

Chen, B. and Gao, H. (2010). An alternative explanantion of the effect of humidity in gecko adhesion: Stiffness reduction enhances adhesion on a rough surface. *Int. J. Appl. Mech.*, **2**(1):1–9.

Gravish, N., Wilkinson, M., and Autumn, K. (2008). Frictional and elastic energy in gecko adhesive detachment. *J. R. Soc. Interface*, **5**(20):339–348.

Hansen, W. R. and Autumn, K. (2005). Evidence for self-cleaning in gecko setae. *Proc. Natl. Acad. Sci. USA*, **102**(2):385–389.

Hill, G. C., Soto, D. R., Peattie, A. M., Full, R. J., and Kenny, T. W. (2011). Orientation angle and the adhesion of single gecko seta. *J. R. Soc. Interface*, **8**(60):926–933.

Huber, G., Mantz, H., Spolenak, R., Mecke, K., Jacobs, K., Gorb, S. N., and Arzt, E. (2005). Evidence for capillarity contributions to gecko adhesion from single spatula nanomechanical measurements. *Proc. Natl. Acad. Sci. USA*, **102**(45):16293–16296.

Huber, G., Orso, S., Spolenak, R., Wegst, U. G. K., Enders, S., Gorb, S. N., and Arzt, E. (2008). Mechanical properties of a single gecko seta. *Int. J. Mater. Res.*, **99**(10):1113–1118.

Israelachvili, J. N. (1991). *Intermolecular and Surface Forces.* Academic Press, 2nd edition.

Kendall, K. (1975). Thin-film peeling – the elastic term. *J. Phys. D: Appl. Phys.*, **8**:1449–1452.

Kwaki, J. S. and Kim, T. W. (2010). A review of adhesion and friction models for gecko feet. *Int. J. Precis. Eng. Manuf.*, **11**(1):171–186.

Laursen, T. A. (2002). *Computational Contact and Impact Mechanics: Fundamentals of modeling interfacial phenomena in nonlinear finite element analysis.* Springer.

Pugno, N. M. and Lepore, E. (2008). Observation of optimal gecko's adhesion on nanorough surfaces. *Biosystems*, **94**(3):218–222.

Puthoff, J. B., Prowse, M. S., Wilkinson, M., and Autumn, K. (2010). Changes in materials properties explain the effects of humidity on gecko adhesion. *J. Exp. Biol.*, **213**(21):3699–3704.

Reissner, E. (1972). On one-dimensional finite-strain beam theory: The plane problem. *J. Appl. Math. Phys*, **23**:795–804.

Rizzo, N. W., Gardner, K. H., Walls, D. J., Keiper-Hrynko, N. M., Ganzke, T. S., and Hallahan, D. L. (2006). Characterization of the structure and composition of gecko adhesive setae. *J. R. Soc. Interface*, **3**:441–451.

Sauer, R. A. (2006). *An atomic interaction based continuum model for computational multiscale contact mechanics.* PhD thesis, University of California, Berkeley, USA.

Sauer, R. A. (2009). Multiscale modeling and simulation of the deformation and adhesion of a single gecko seta. *Comp. Meth. Biomech. Biomed. Engng.*, **12**(6):627–640.

Sauer, R. A. (2010). A computational model for nanoscale adhesion between deformable solids and its application to gecko adhesion. *J. Adhes. Sci. Technol.*, **24**:1807–1818.

Sauer, R. A. (2011a). Challenges in computational nanoscale contact mechanics. In Müller-Hoeppe, D., Löhnert, S., and Reese, S., editors, *Recent Developments and Innovative Applications in Computational Mechanics.* Spinger.

Sauer, R. A. (2011b). Enriched contact finite elements for stable peeling computations. *Int. J. Numer. Meth. Engrg.*, **87**:593–616.

Sauer, R. A. (2011c). The peeling behavior of thin films with finite bending stiffness and the implications on gecko adhesion. *J. Adhes.*, **87**(7-8):624–643.

Sauer, R. A. (2012a). Computational contact formulations for soft body adhesion. In Li, S. and Sun, B., editors, *Advances in Soft Matter Mechanics.* Spinger.

Sauer, R. A. (2012b). A geometrically exact finite beam element formulation for thin film peeling. *in preparation.*

Sauer, R. A. and Holl, M. (2012). A detailed 3D finite element analysis of the peeling behavior of a gecko spatula. *Comp. Meth. Biomech. Biomed. Engng.*, DOI: 10.1080/10255842.2011.628944.

Sauer, R. A. and Li, S. (2007). A contact mechanics model for quasi-continua. *Int. J. Numer. Meth. Engrg.*, **71**(8):931–962.

Sauer, R. A. and Li, S. (2008). An atomistically enriched continuum model for nanoscale contact mechanics and its application to contact scaling. *J. Nanosci. Nanotech.*, **8**(7):3757–3773.

Sauer, R. A. and Wriggers, P. (2009). Formulation and analysis of a 3D finite element implementation for adhesive contact at the nanoscale. *Comput. Methods Appl. Mech. Engrg.*, **198**:3871–3883.

Simo, J. C. (1985). A finite strain beam formulation. The three-dimensional dynamic problem. Part I. *Comput. Meth. Appl. Mech. Engrg.*, **49**:55–70.

Simo, J. C. and Vu-Quoc, L. (1986). A three-dimensional finite strain rod model. Part II: Computational aspects. *Comput. Meth. Appl. Mech. Engrg.*, **58**:79–116.

Sun, W., Neuzil, P., Kustandi, T. S., Oh, S., and Samper, D. (2005). The nature of the gecko lizard adhesive force. *Biophys. J.*, **89**(2):L14–L17.

Wriggers, P. (2006). *Computational Contact Mechanics*. Springer, 2nd edition.

Wriggers, P. (2008). *Nonlinear Finite Element Methods*. Springer.

Wriggers, P. and Reinelt, J. (2009). Multi-scale approach for frictional contact of elastomers on rough rigid surfaces. *Comput. Methods Appl. Mech. Engrg.*, **198**(21-26):1996–2008.